Redox Biology 37 (2020) 101727

Contents lists available at ScienceDirect

Redox Biology

journal homepage: www.elsevier.com/locate/redox

Research Paper

The correlation of IRE1α oxidation with Nox4 activation in aging-associated vascular dysfunction

Hwa-Young Lee [a,b,1], Hyun-Kyoung Kim [e,1], The-Hiep Hoang [a,b], Siyoung Yang [c], Hyung-Ryong Kim [d], Han-Jung Chae [b,e,*]

[a] Department of Pharmacology and Institute of New Drug Development, Jeonbuk National University Medical School, Jeonju, Jeonbuk, 54907, Republic of Korea
[b] Non-Clinical Evaluation Center Biomedical Research Institute, Jeonbuk National University Hospital, Jeonju, Jeonbuk, 54907, South Korea
[c] Department of Pharmacology, Ajou University School of Medicine, Suwon, 16499, Republic of Korea
[d] College of Dentistry, Dankook University, Cheonan, 152, Republic of Korea
[e] School of Pharmacy, Jeonbuk National University, Jeonju, Jeonbuk, 54907, Republic of Korea

ARTICLE INFO

Keywords:
Oxidative stress
NADPH oxidase 4
Reactive oxygen species
Endoplasmic reticulum
Vascular dysfunction

ABSTRACT

Oxidative stress attributable to the activation of a Nox4-containing NADPH oxidase is involved in aging-associated vascular dysfunction. However, the Nox4-induced signaling mechanism for the vascular alteration in aging remains unclear. In an aged aorta, the expression of Nox4 mRNA and protein by Nox family of genes was markedly increased compared with a young aorta. Nox4 localization mainly to ER was also established. In the aorta of Nox4 WT mice aged 23–24 months (aged), reactive oxygen species (ROS) and endoplasmic reticulum (ER)/oxidative stress were markedly increased compared with the counter KO mice. Furthermore, endothelial functions including eNOS coupling process and acetylcholine-induced vasodilation were significantly disturbed in the aged WT, slightly affected in the counter KO aorta. Consistently, in D-galactose-induced *in vitro* aging condition, ER-ROS and its associated ER Nox4 expression and activity were highly increased. Also, in chronic D-galactose-treated condition, IRE1α phosphorylation and XBP-1 splicing and were transiently increased, but IRE1α sulfonation was robustly increased in the aging Nox4 WT condition when compared to the counter KO condition. *In vitro* D-gal-induced aging study, the phenomenon were abrogated with Nox4 knock-down condition and was significantly decreased in GKT, Nox4 inhibitor and 4-PBA, ER chemical chaperone-treated human umbilical vein endothelial cells. The state of Nox4-based ER redox imbalance/ROS accumulation is suggested to determine the pathway "the UPR; IRE1α phosphorylation and XBP-1 splicing and the UPR failure; IRE1α cysteine-based oxidation, especially sulfonation, finally controlling aging-associated vascular dysfunction.

1. Introduction

Age is recognized as a major risk factor for cardiovascular diseases. Since many age-related cardiovascular and cerebrovascular diseases develop due to either alteration in arterial function or are aggregated by arterial functional and phenotypic changes, thus, it is important to have a better understanding on the mechanisms that underlie arterial aging [1]. As such, aging-induced functional and structural alterations of the microcirculation contribute to the pathogenesis of a range of age-related diseases, including atherosclerosis, stroke, diabetes, and glaucoma, affecting millions of people worldwide. Vascular oxidative stress increases with age as a consequence of increased production of reactive oxygen species (e.g. superoxide). Sources of increased superoxide production include upregulation of the oxidant enzyme NADPH oxidase and uncoupling of the normally NO-producing enzyme, eNOS (endothelial NO synthase).

This observation indicates a strong correlation between aging and oxidative stress, resulting in the development of endothelial/vascular dysfunction [2]. An early feature in the development of cardiovascular diseases is the progressive endothelial dysfunction attributable to increased reactive oxygen species (ROS) production by a Nox4-containing NADPH oxidase [3]. Oxidative stress causes DNA damage, alters transcriptional machinery, and promotes inflammatory gene expression. All these are key factors that further accelerate vascular

* Corresponding author. School of Pharmacy, Jeonbuk National University, Jeonju, Jeonbuk, 54907, Republic of Korea.
E-mail address: hjchae@jbnu.ac.kr (H.-J. Chae).
[1] These authors contributed equally.

https://doi.org/10.1016/j.redox.2020.101727
Received 5 June 2020; Received in revised form 10 September 2020; Accepted 11 September 2020
Available online 14 September 2020

aging [3]. Mechanisms regulating these functions are unclear, but may be related to Nox4, ROS, post-translational oxidative modification of signaling proteins, and interaction with stress response processes, such as endoplasmic reticulum (ER) stress [4].

The endoplasmic reticulum (ER) is a subcellular organelle in eukaryotic organisms that plays a role in structural modifications of proteins, which are essential for its proper functions. However, accumulation of unfolded or misfolded proteins in the ER lumen triggers ER stress [5], which ultimately causes several pathological disorders, many of which have implications for aging, such as cardiovascular diseases [6]. In response to ER stress, inositol-requiring kinase/endonuclease-1 alpha (IRE1α) catalyzes cleavage of a small intronic segment from the unspliced X-box protein 1 (uXBP-1) gene, yielding the spliced form of XBP-1 (sXBP-1), whose translation produces an active transcription factor. Based on this information, sXBP-1 transcript levels are widely used as an ER stress indicator [7].

Reactive oxygen species (ROS) have been implicated in a variety of pathological conditions [8]. Oxidative stress can also influence the function of organelles, such as ER which is a major site of protein synthesis, lipid biosynthesis, and Ca^{2+} storage and signaling [9]. Hence, alterations in the ER can have an impact on the cell's function and fate. The ER responds to accumulation of misfolded proteins by activating the unfolded protein response (UPR). This complex signaling network can restore ER homeostasis and also promotes cell survival or apoptosis [10]. ER stress is defined by "hyper ER folding load state, and related misfolded protein accumulation" [11], but not ER stress responses, i.e., UPR. The ER stress includes general ER stress characterized by elevated levels of ROS and calcium among other events [11,12]. Once generated, ROS influence signaling molecules through post-translational oxidative modification of proteins [13].

Cellular functional responses are influenced by oxidation status and majority forms of reversible oxidation include adjustment of cysteine to sulfenic acid (sulfenylation, SOH), reaction with glutathione (glutathionylation), and formation of disulfide bonds [14]. Reversible cysteine oxidation is key to redox signaling, providing a mechanism of redox switch for protein function as well as cell function. In pathological conditions, high concentrations of ROS can result in irreversible oxidation, such as protein carbonylation (modification of amino acid side chains to carbonyl derivatives), and formation of sulfenic and sulfonic acid on cysteine residues (SO_2H, SO_3H), resulting in protein damage, degradation, and cell death [15]. Also, high levels of ROS cause damage to the proteins, a growing body of evidence suggests that ROS also have physiological signaling functions that are mediated through oxidation of specific Cysteine residues [16]. Redox-imbalance is ultimately linked to ROS, which induces inappropriate protein modification and abnormal protein function. The "ER stress" plays a key role in several human diseases, including metabolic disease, neurodegenerative disease, inflammatory disease, neoplasms, as well as pathologies of the heart, kidney, and lung [17–19]. However, the relationship between oxidative stress and ER stress and the interaction between these processes in vascular dysfunction in aging are unknown.

This study shows that Nox4-derived ROS control ER stress-eNOS uncoupling axis that is based on IRE1α oxidation via "IRE1α sulfonation". The Nox4-IRE1α status explains age-associated vascular dysfunction, suggesting an anti-aging molecular mechanism for vascular health.

2. Materials and methods

2.1. Reagents

D-galactose (G0750), 4-phenylbutyric acid (4-PBA, P21005), and tunicamycin (T7765) were purchased from Sigma Aldrich (St Louis, MO, USA). GKT137831 were purchased from Cayman Chemical (1218942-37-0, Ann Arbor, MI, USA). Cell culture media and antibiotics were obtained from Lonza and Gibco. Fluorescent probes and secondary antibodies coupled to fluorescent markers were purchased from Molecular Probes, Invitrogen. All other reagents were obtained from Sigma or the highest grade available.

2.2. Animal studies

This study was carried out strictly following the recommendations in the Guide for the Care and Use of Laboratory Animals of the Jeonbuk National University. Animal protocols were approved by the Committee on the Ethics of Animal Experiments of the Jeonbuk National University. C57BL/6J mice (Jackson Laboratories, Bar Harbor, ME, USA) and Nox4 KO mice (B6.129-*NOX4tm1Kkr*/J, Jackson Labs) were randomly assigned into three groups of seven animals each and given a standard rodent chow diet. Mice were housed in a 12 h:12 h light: dark cycle with access to food and water ad libitum. Mice were starved overnight before sacrifice. The aorta and blood were frozen at −80 °C for biochemical analysis.

2.3. Cell culture and transfection

Human umbilical vein endothelial cells (HUVECs) were purchased from Lonza (Basel, Switzerland) and were grown in EGM2 culture medium (CC-3162, Lonza) supplemented with 10% fetal bovine serum under 5% CO_2 at 37 °C. Cell transfection was performed using Lipofectamine 3000 (Invitrogen, Carlsbad, CA, USA) according to the manufacturer's instructions.

2.4. Plasmid

IRE1α plasmid was kindly donated by Yong Liu (University of the Chinese Academy of Sciences, China). The point mutants of IRE1α were generated using Muta-Direct™ Site-Directed Mutagenesis Kit (15071, Biotechnology, Seongnam-Si, Republic of Korea) according to the manufacturer's protocols. All constructs were confirmed by DNA sequencing.

2.5. Western blot and immunoprecipitation

Cells were lysed with lysis buffer (20 mM Tris, pH 7.4, 150 mM NaCl, and 0.5% Triton X-100) or RIPA buffer (150 mM NaCl, 50 mM Tris, pH 8.0, 2 mM EDTA, 1% Nonidet P-40, and 0.1% SDS) supplemented with a protease and phosphatase inhibitors (78430, 78428, Invitrogen), and lysates were centrifuged at 16,200 g for 30 min at 4 °C. Then, the lysates were used for Western blot analyses. For immunoprecipitation, cells were lysed with IP lysis buffer (50 mM Tris-HCl, pH 8.0, containing 150 mM NaCl, 0.015% phenylmethylsulphonyl fluoride, 1 mM dithiothreitol, 1 mM EDTA, 1% sodium deoxycholate, 1% Triton X-100, and 1% SDS). Primary antibody was coupled with protein A and G beads (P6031, P3296, Sigma), and then, the immune complex was added to the cell lysates and incubated at 4 °C overnight. After immunoprecipitation, the samples were washed with IP lysis buffer for three times. Proteins were eluted with 2xSDS sample buffer. The eluates were subjected to SDS-PAGE, and proteins were detected using the Western ECL Substrate (1705061, Bio-Rad) and Amersham Hyperfilm (28-9068-37, GE Healthcare, Amersham, UK). Sample preparation, Western blot, and determination of eNOS (sc-376751, Santa Cruz) dimer-to-monomer ratio were performed as described previously [20].

2.6. NADPH oxidase activity assay

Nox activity was determined by the lucigenin-enhanced chemiluminescence method [21]. ER microsomes were added to phosphate buffer containing 5 μM lucigenin (M8010, Sigma) and 100 μM NADPH (10107824001, Sigma). Luminescence indicative of Nox-derived ROS production was expressed relative to the total protein content.

2.7. Sulfonylation and Sulfonation

Sulfenylation was performed as described previously [22]. Briefly, cells were lysed in lysis buffer (50 mM HEPES, 50 mM NaCl, 1 mM EDTA, 10% glycerol, 1% Triton X-100) supplemented with 1 mM DCP-Bio1 (EE0028, Kerafast, Boston, MA, USA), 0.1 mM N-Ethylmalemide, 0.1 mM iodoacetamide and protease inhibitors. Samples were kept in ice for 30 min sonication and centrifuged at 12,000 g for 20 min at 4 °C. The supernatant was transferred to a tube and rotated for 1 h at room temperature to allow for labeling of sulfonic acids. After incubation, protein was precipitated by acetone and centrifuged at 12,000 g for 5 min. The pellet was washed by 70% acetone and suspended in a non-supplemented lysis buffer. 1 mg of total protein was added to 50 μL slurry of streptavidin beads. Then, beads were rotated overnight at 4 °C. After 24 h, beads were centrifuged at 1000 g for 3 min, supernatant was discarded and beads were washed with 1 mL of lysis buffer. This washing step was repeated three times and beads were eluted in 30 μL of reducing 2 × LDS buffer (Life Technologies). For detection of sulfonation, anti--sulfonate antibody (ab176487, Abcam, Cambridge, MA, USA) was applied.

2.8. ROS measurement

For ROS detection, DCFDA Cellular ROS Assay Kit (ab113851, Abcam) was used and measured according to the manufacturer's manual.

2.9. Immunofluorescence microscopy

Cells were seeded on a confocal dish rinsed in PBS, fixed in methanol for 10 min, and then permeabilized using 0.1% Triton X-100 in 1xPBS with 30 min. The cells were blocked with 5% BSA (Sigma) for 1 h and then incubated overnight at 4 °C with the primary antibody. After washing twice in PBS, cells were incubated for 1 h with a cocktail of secondary antibodies including Donkey Anti-Mouse conjugated to tetramethylrhodamine isothiocyanate (T5393, TRITC, 1:100; Sigma) and Donkey Anti-Rabbit conjugated to FITC (F0382, 1:100; Sigma) diluted in blocking solution. Appropriate washing in PBS was performed between each step, and incubation was performed in a dark, moist chamber at room temperature. The sections were mounted with VECTASHIELD (Vector Laboratories). Images were obtained on DeltaVision Microscopy Imaging System (Applied Precision, Issaquah, WA, USA).

2.10. HyPer-red ER and HyPer-Red mito live cell imaging

Cells were seeded onto a confocal dish (SPL, Life Sciences, Seoul, Korea) and transiently transfected with HyPer-Red ER constructs using Lipofectamin 3000. The cells were washed twice in PBS and then cell were stained with Hoechst 33342 for 3 min. Images were obtained on DeltaVision Microscopy Imaging System (Applied Precision, Issaquah, WA, USA).

2.11. IRE1α foci cell imaging

Analysis of IRE1α foci formation was carried out as previously described [23]. Briefly, HUVECs were transiently transfected with IRE1α-GFP expression for 24 h. Fluorescent microscopic images were taken with DeltaVision. Foci-positive was calculated as the number of cells with one or more foci out of total number of cells.

2.12. RNA isolation

Sample collection and preparation for RNA sequencing were done using 2 months' (young) and 23–24 months' (aging) Nox4 WT, which were sacrificed by CO_2 inhalation, and thoracic aortas were extracted, cleaned of fatty tissue, and digested with 2 mg/mL collagenase (CLS-2, Worthington) for 10 min at 37 °C to separate medial and adventitial tissue. Total RNA was isolated using TRIzol reagent (15596026, Thermo Fisher Scientific, Waltham, MA, USA). RNA quality was assessed by Agilent 2100 Bioanalyzer (Agilent Technologies, Amstelveen, The Netherlands), and ND-2000 Spectrophotometer (Thermo Inc., DE, USA) was used for RNA quantification.

2.13. Library preparation and sequencing

For control and test RNAs, the construction of library was performed using QuantSeq 3'mRNA-Seq Library Prep Kit (016.96, Lexogen, Inc., Austria) according to the manufacturer's instructions. In brief, each 500 ng total RNA were prepared and an oligo-dT primer containing an Illumina-compatible sequence at its 5'end was hybridized to the RNA and reverse transcription was performed. After degradation of the RNA template, second strand synthesis was initiated by a random primer containing an Illumina-compatible linker sequence at its 5'end. The double-stranded library was purified using magnetic beads to remove all reaction components. The library was amplified to add the complete adapter sequences required for cluster generation. The finished library was purified from PCR components. High-throughput sequencing was performed as single-end 75 sequencing using NextSeq 500 (Illumina, Inc., USA).

2.14. Lucigenin-enhanced chemiluminescence assay for superoxide production

For superoxide measurement, we followed the previously described procedure [24].

2.15. Subcellular fractionation

Cellular or aorta ring fractionation was performed as previously reported [25]. The total homogenate was centrifuged for 10 min at 1000 *g* and the supernatant was centrifuged twice at 9000 g to pellet crude mitochondria and twice at 7000 g and once at 10,000 g for cells. The supernatant was centrifuged at 20,000 g for 30 min, after which the resulting supernatant was further centrifuged at 100,000 g to give a supernatant (cytosol) and a pellet (ER).

2.16. Analyses of lipid peroxidation

Lipid peroxidation was quantified in whole lysate and ER fraction lysates using a lipid hydroperoxide assay kit (705002, Cayman Chemicals, Ann Arbor, MI, USA). In this assay, lipid hydroperoxide was extracted from the samples into chloroform using the extraction buffer provided by the manufacturer. The chromogenic reaction was carried out at room temperature for 5 min, and the absorbance of each well was measured at 500 nm using a 96-well plate spectrometer (SpectraMax 190, Molecular Devices, Sunnyvale, CA, USA), using 13-hydroperoxy-octadecadienoic acid as the standard. The cellular levels of lipid hydroperoxide were calculated as described by the manufacturer.

2.17. Tissue histology, immunohistochemistry, and immunofluorescence

Mice were dissected, aortas were fixed with 4% formaldehyde in PBS and embedded in paraffin. For paraffin-embedded specimens (thoracic aorta), 4 μM sections were prepared. H&E staining was used for morphological examination. Paraffin-embedded sections of aorta were rehydrated, and recovery of antigen was achieved by heating in a medium containing 10 mM sodium citrate and 0.05% Tween 20 at pH 6.2. Antibodies used in tissue immunohistochemistry were rabbit polyclonal anti-Nox4 (NB110-58851, Novus Biologicals, United Kingdom) and rabbit polyclonal anti-β-galactosidase (ab4761, Abcam), followed by incubation with secondary antibody (conjugated to horseradish peroxidase-labeled polymer) in PBS and 1% BSA. Bound antibodies were

visualized by 5 min incubation with liquid 3,3′-diaminobenzidine substrate chromogen. Finally, sections were counterstained in Mayer's hematoxylin, mounted, and evaluated under light microscope. Immunofluorescence was performed following a standard protocol. Sections were washed with PBS, blocked in blocking solution (Code X0909, Dako, Glostrup, Denmark), and the primary antibodies were added to the slides and incubated overnight in a humified chamber at 4 °C. Afterward, sections were washed and incubated in secondary antibodies diluted in blocking buffer for 1 h at RT, washed again and mounted with FluorSave (EMD Millipore). Antibody used in tissue immunofluorescence is rabbit monoclonal anti-p-eNOS Ser1177 (9570S, Cell Signaling Technology, Danvers, MA USA) and observed under a fluorescence microscope. The fluorescence signal intensity was analyzed using Image J software (National Institutes of Health, Bethesda, MD, USA).

2.18. Statistical analysis

GraphPad Prism 6 software (GraphPad Software, San Diego, CA, USA) was used for all statistical analyses. Differences between experimental and control groups were determined by unpaired two-tailed Student's *t*-test (where two groups of data were compared) or two-way ANOVA analysis (where more than two groups of data were compared). *P*-value less than 0.05 was considered statistically significant.

3. Results

3.1. Nox4 expression in aged aortic vascular endothelial cells activates vascular dysfunction and endoplasmic reticulum (ER) stress

To examine the vascular endothelial function of Nox4, we generated transgenic mice that were young (2-month) or aged Nox4 (23–24-month) wild type (WT) or knockout (KO) to study the *in vivo* role of Nox4 (Supplementary Fig. S1A and B). Vascular dysfunction is a hallmark of aging [26], although how this impacts the vascular endothelial function is not clear. To study the effect of Nox4 on various biological function gene sets, we analyzed expression profiles conducting RNA-seq-based transcriptome analysis, and the differential expressions of UPR-related gene and oxidative stress-related genes were significantly elevated in aged Nox4 WT mice compared with young Nox4 WT including Nox4, Cyba, Sod3, Dnajb2 and Ppia (Fig. 1A). Next, as aging is associated with vascular oxidative stress and vascular endothelial senescence, we performed gene ontology related to oxidative stress and cell metabolism. DAVID KEGG enrichment analysis revealed strong enrichment of oxidative stress pathways, including oxidation-reduction process, ROS metabolic process, superoxide anion generation signaling pathway, and endoplasmic reticulum stress signaling pathway (Fig. 1B). NOX enzymes comprise a family of NADPH dependent oxidoreductases [27]. So we predicted relative NOX4 in aging-induced vascular endothelial dysfunction. As expected, Nox4 expression was increased in aged Nox4 WT mice (Fig. 1C). To evaluate whether Nox4 regulation is compartment-specific in vascular senescence, we investigated the subcellular localization of Nox4. Nox4 levels were significantly increased in the ER of aorta (Fig. 1D and E). These findings indicate that Nox4 is

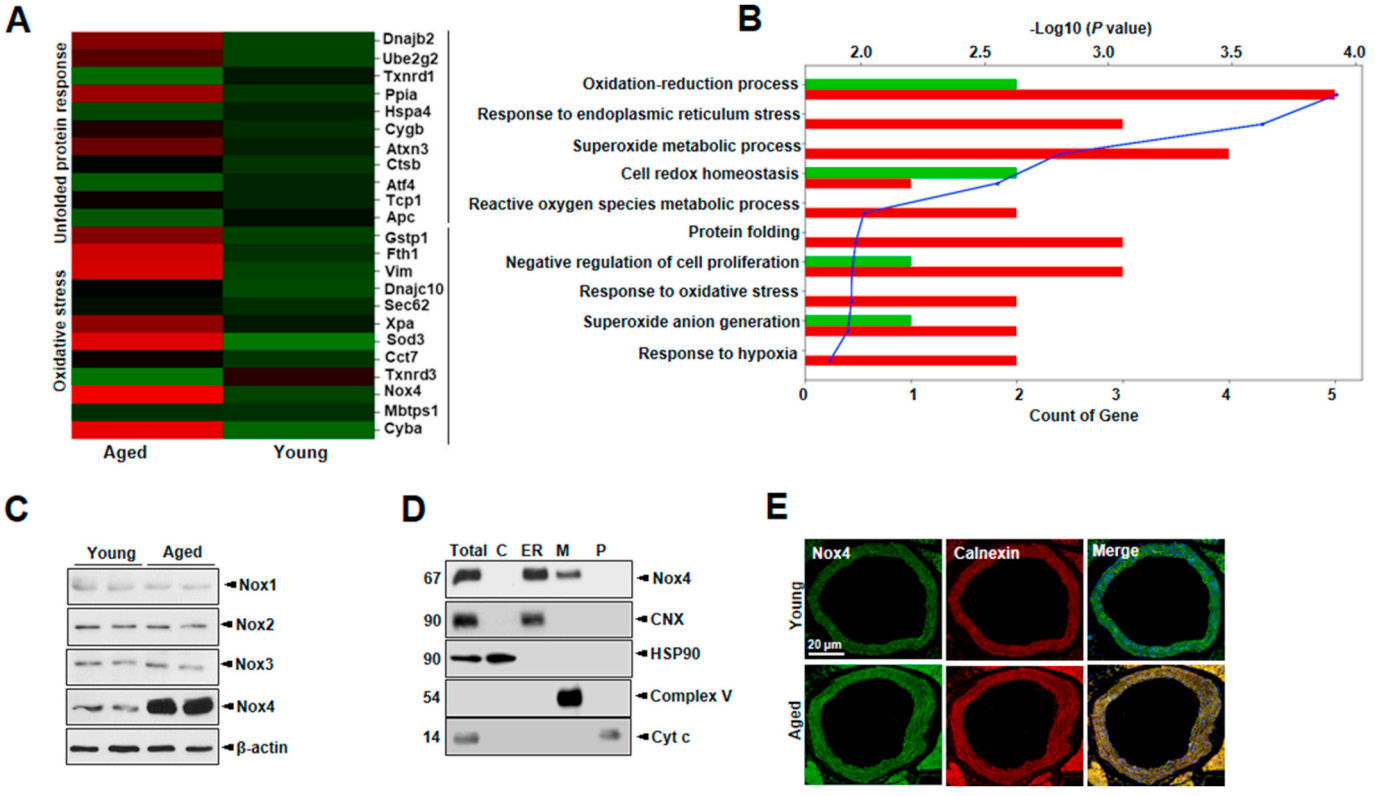

Fig. 1. Nox4 expression in vascular endothelial cells in aorta activates endoplasmic reticulum (ER) stress and unfolded protein response (UPR). Aortas from young (2-month) Nox4 WT, KO and aged (23- to 24-month) Nox4 WT, KO mice ($n = 7$ animals per group). (A) Bioinformatic analysis was performed in aortas from aged Nox4 WT mice and young Nox4 WT mice by the heatmap. (B) KEGG enrichment analysis showing repressed signaling pathways from aged Nox4 WT mice and young Nox4 WT mice. (C) Western blots analysis of Nox1, Nox2, Nox3, Nox4, and β-actin expression in young and aged aorta tissues. (D) Lysates were processed to obtain subcellular fractions and analyzed by Western blot. (E) Confocal images (scale bars, 20 μm) show localization of Nox4 (red) to the ER, which was labeled with an *anti*-calnexin antibody (green). Yellow dots denote the co-localization of Nox4 and calnexin signals. Cell nuclei were stained with DAPI (blue). (For interpretation of the references to colour in this figure legend, the reader is referred to the Web version of this article.)

expressed in subcellular compartments, especially in the ER.

3.2. Nox4 activates aging-associated oxidative stress and endothelial dysfunction

To examine the interplay of ROS, aging, and vascular dysfunction, we first determined the senescence by measuring biomarkers of cellular senescence, including senescence-associated-β-galactosidase (SA-β-gal) expression in aortas from young and aged Nox4 WT and Nox4 KO mice. The expression of SA-β-gal increased remarkably in aged Nox4 WT group compared to the aged Nox4 KO group (Supplementary Fig. S2A). We hypothesized that Nox4 overexpression increased vascular hypertrophy because of Nox4-induced vascular oxidative stress. To validate this hypothesis, we quantified aortic hypertrophy from young and aged Nox4 WT and Nox4 KO mice. As expected, vascular hypertrophy was increased in aged Nox4 WT mice; however, the aged Nox4 KO mice had significantly diminished vascular hypertrophy (Supplementary Fig. S2B). Also, aortic wall thickness was significantly reduced in aged Nox4 KO mice compared to the aged Nox4 WT mice (Supplementary Fig. S2C). These data support the pathophysiological role of Nox4 depletion in vascular hypertrophy. It was also observed that endothelial-dependent relaxation was impaired in aged Nox4 WT mice compared to the KO mice (Fig. 2A). Considering that impairment of NO production is a hallmark of endothelial aging [28], DAF-2DA probe was used to detect endothelial NO production [29]. As shown in Fig. 2B, the fluorescence intensity of NO was reduced in aged Nox4 WT mice but was reversed in Nox4 KO mice. Modulation of NO bioavailability was also assessed via analysis of eNOS expression and its phosphorylation status. Activated eNOS is characterized by phosphorylation at serine 1177 [30]. The phosphorylation level is significantly decreased in aged Nox4 WT mice compared with KO mice (Fig. 2C). Finally, the percentage of dimer-to-monomer ratio, an indicator of eNOS uncoupling [31,32] was significantly decreased in aged Nox4 WT mice, which was reversed by the counter KO mice (Fig. 2D). Vascular oxidative stress can cause decreased NO bioavailability, leading to endothelial dysfunction [33]. Increased ROS production in the aging aorta was further examined *in situ* by DHE fluorescence in aortic sections (Fig. 2E). There was a significant increase in DHE fluorescence throughout the aortic wall of aged Nox4 WT mice compared to young Nox4 WT mice vessels, which is also more significant than that of the aged KO mice. Since oxidative stress may be linked to ER-associated ROS [34], we assessed intra-ER NADPH oxidase activity, hydrogen peroxide, and membrane lipid peroxidation in aged Nox4 or young mice. The increase in NADPH oxidase activity, hydrogen peroxide, and membrane lipid peroxidation observed in aged Nox4 WT mice was reduced by the aged Nox4 KO aortas (Fig. 2F–H). Additionally, we determined the levels of ER stress markers (Fig. 2I). The levels of ER stress markers (p-IRE1α, *p*-eIF2α, ATF4, and CHOP) were markedly elevated in the aged Nox4 WT mice compared with aged Nox4 KO mice. It's thus suggested that Nox4 depletion is able to preserve the reduction of NO production and oxidative stress, where ER redox imbalance and resultant ER stress are involved.

3.3. D-gal accelerates vascular aging and senescence, promoting age-dependent oxidative stress and endothelial dysfunction

Oxidative stress-induced premature endothelial senescence is also characterized by DNA damage and telomere dysfunction [35]. To investigate the effect on endothelial senescence, endothelial telomerase activity, which indicates replicative senescence, was significantly decreased with D-gal in HUVECs (Fig. 3A). Treatment of GKT or 4-PBA inhibited the decrease of telomerase activity in the D-gal-treated condition. D-gal significantly upregulated the expressions of SA-β-gal, p21, and p16 (Fig. 3B). The upregulation of these senescence markers was attenuated by GKT, Nox inhibitor or 4-PBA, ER chaperone. Consistently, the D-gal-enhanced the proportion of SA-β-gal-positive cells, which were significantly inhibited by either GKT or 4-PBA (Fig. 3C). In Fig. 3D, the fluorescence intensity of NO was shown to be reduced by D-gal treatment but was reversed by GKT or 4-PBA treatment. In senescent HUVECs induced by D-gal, the phosphorylation level was significantly decreased (Fig. 3E). Treatment of GKT or 4-PBA rendered the rebound of *p*-Ser1177. To determine whether vascular endothelial senescence observed in the aging model is mediated by increased oxidative stress, we measured general ROS or protein oxidation levels. D-gal significantly increased all of the oxidative stress markers as compared to control cells (Fig. 3F and G). Since protein oxidation may be linked to ER-associated ROS [36], we assessed intra-ER ROS, NADPH oxidase activity, or lipid peroxidation status and by measuring H_2O_2 production and the GSH/GSSG ratio in HUVECs with D-gal-induced endothelial senescence with and without GKT or 4-PBA treatment. To quantify H_2O_2 levels in the ER, we used the protein-based reporter molecule "HyPer" [37]. HyPer consists of a circularly permuted red fluorescent protein (cpRFP) inserted into the H_2O_2-sensitive regulatory domain of the *E. coli* transcription regulator OxyR. This construct is also pH-sensitive. Therefore, we mutated a critical HyPer cysteine residue (C199S) to obtain the biosensor "SypHer", which is H_2O_2-insensitive and can be used as a HyPer control [38–40]. In the D-gal-treated cells of the *in vitro* aging model, intra-ER ROS levels were highly increased, which were abrogated by GKT or 4-PBA (Fig. 3H and Supplementary Figs. S3A–C). Nox activity in ER fraction was significantly increased by D-gal treatment, which was significantly reduced in the presence of GKT or 4-PBA (Supplementary Fig. S3D). H_2O_2 production and lipid peroxidation levels in the ER fraction were also increased in D-gal treatment compared to control cells, which were reduced in the presence of GKT or 4-PBA (Supplementary Figs. S3E and F). The balance between GSH and GSSG in the ER reflects ER protein oxidation status [41]; we observed that the GSH:GSSG ratio was decreased in D-gal treatment and restored by GKT and 4-PBA treatment (Supplementary Fig. S3G). ER stress-induced ROS generation impairs protein folding that disrupts ER functioning. To confirm the redox status of protein disulfide isomerase (PDI), D-gal treatment condition was exposed to diamide oxidative agent [42]. The oxidized form of PDI was readily converted to the reduced form of PDI under washout conditions with control but persisted in D-gal exposed samples. Interestingly, this was recovered by the presence of GKT or 4-PBA in the washout condition (Supplementary Fig. S3H), suggesting that NADPH oxidases 4 might contribute to the aging-associated increase in vascular oxidative stress [43]. We also investigated whether Nox4 is involved in aging-associated vascular senescence. Indeed, expression of Nox4 was markedly enhanced in dose-dependent D-gal treatment (Supplementary Fig. S3I). In contrast, Nox4 protein expression was decreased with GKT or 4-PBA treatment. To evaluate whether Nox4 regulation is compartment-specific in vascular senescence, we investigated the subcellular localization of Nox4. Nox4 levels were significantly increased only in the ER of HUVECs (Supplementary Figs. S3J and K). These findings indicate that Nox4 is expressed in subcellular compartments, especially in the ER. This is a highly regulated process since all the ROS-generating organelles do not possess Nox4. The ER is a site of protein synthesis and a platform of stress signaling pathways that may be particularly important in oxidative stress in vascular senescence and was further investigated in these studies.

3.4. Irreversible oxidation of IRE1α by NADPH oxidase 4-originated dynamic ROS influences vascular injury

Based on our findings of increased Nox4 content in the ER in vascular senescence, we probed for the potential interaction between Nox4, ROS, and ER and the possibility that Nox4-derived ROS may influence ER function and ER stress. Remarkably, low-dose D-gal treatment induced the IRE1α-mediated response to ER stress as indicated by IRE1α phosphorylation, XBP-1 mRNA splicing, and GRP78 expression (Supplementary Figs. S4A and B). The phosphorylation of the UPR mediators PERK and IRE1α as well as expression of the ATF4 and CHOP involved in

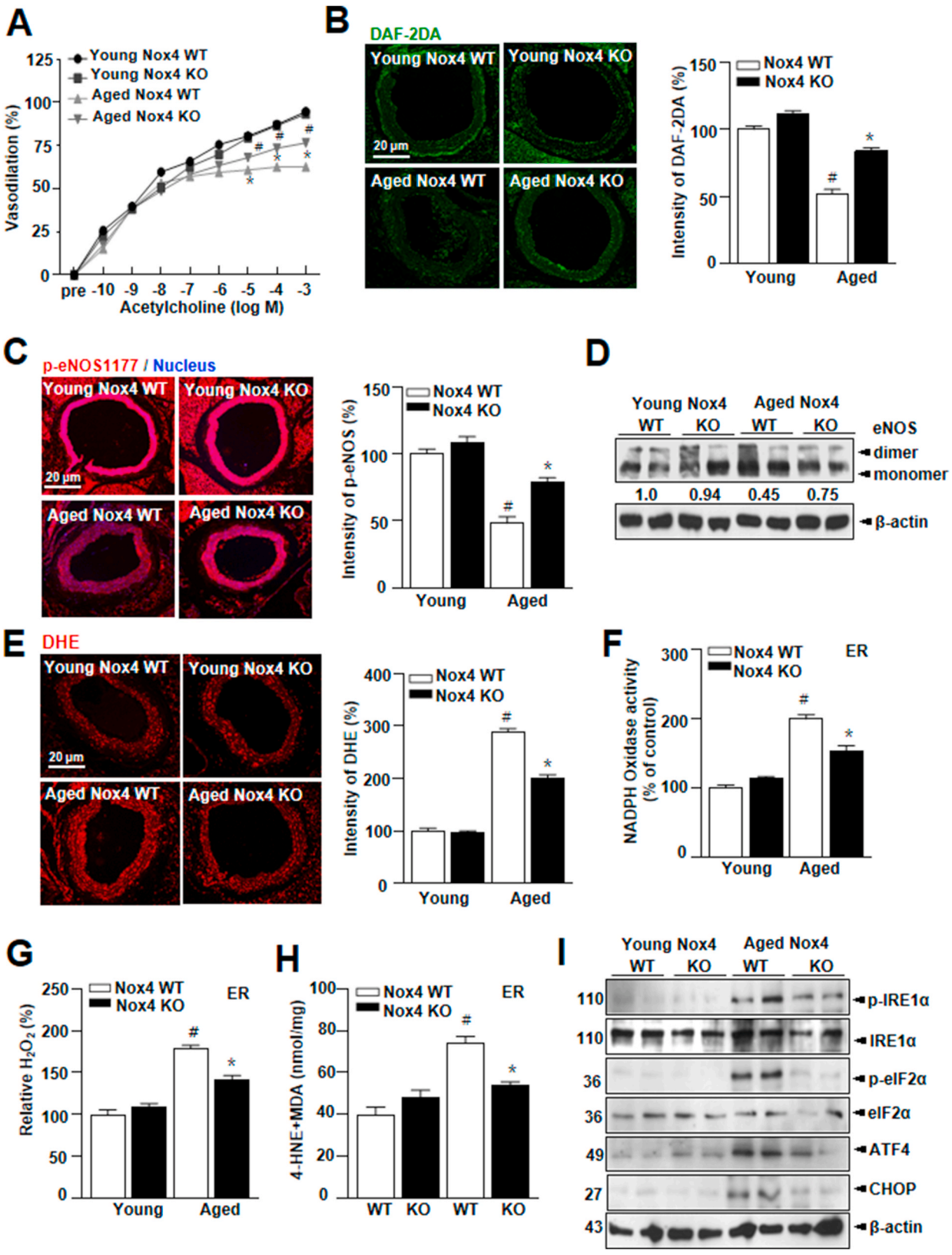

Fig. 2. Nox4 activates aging-associated oxidative stress and endothelial dysfunction. Aortas from young (2-month) Nox4 WT, KO and aged (23- to 24-month) Nox4 WT, KO mice. ($n = 7$ animals per group) (A) Endothelial-dependent vasodilation to acetylcholine. Representative aortic sections (scale bars, 20 μm) were stained for DAF-2DA (B), *p*-eNOS (ser 1177) (C). Immunoblotting analysis of eNOS-dimers and -monomers in the young and aged aorta (D). Representative aortic sections(scale bars, 20 μm) were stained for DHE (E). Lysates from aorta tissues were analyzed for NADPH oxidase activity (E), hydrogen peroxide level (F), 4-HNE-malondialdehyde (MDA) level (G) in the aorta ER fraction. (H) Western blots analysis of p-IRE1α, IRE1α, *p*-eIF2α, eIF2α, ATF4, GRP78, CHOP, and β-actin expression in aorta tissues. ($n = 7$ animals per experimental group). Data are mean ± standard deviation. $^{\#}$, $p < 0.05$; *, $p \leq 0.01$.

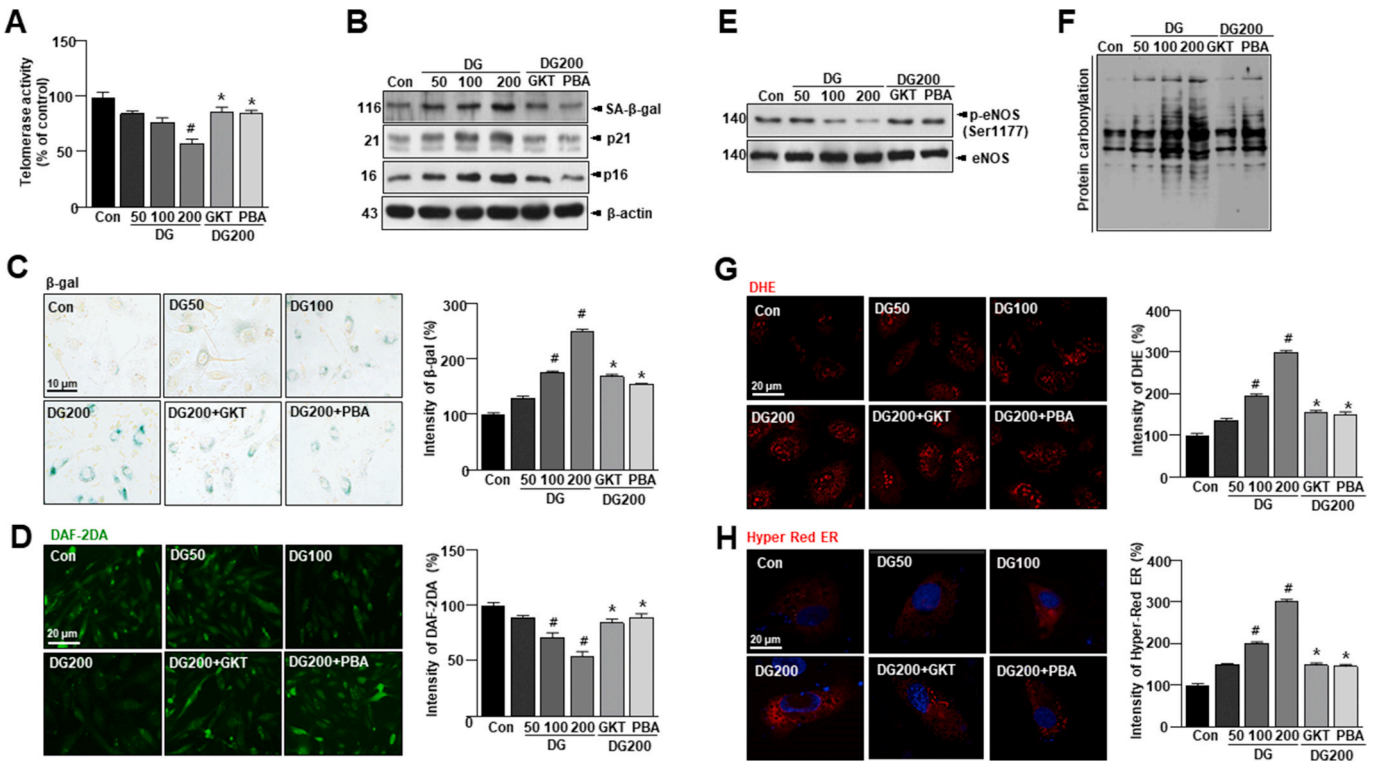

Fig. 3. D-gal accelerates vascular aging and senescence, promoting age-dependent oxidative stress and endothelial dysfunction. HUVECs were treated with 10 μM GKT137831 or 5 mM 4-PBA with or without 50, 100, or 200 mM D-gal for 24 h. (A) Telomerase activity was performed in HUVECs. (B) Western blots analysis of SA-β-gal, p21, p16, and β-actin expression in aorta tissues. (C) Representative senescence-associated β-galactosidase (SA-β-gal) staining in HUVECs. (D) Representative fluorescent images of NO formation in HUVECs were shown using NO probe DAF-2DA. (E) Western blots of *anti*-phospho-eNOS Ser1177 or total-eNOS antibody were performed in HUVECs. (F) Lysates from aorta tissues were analyzed for oxidized proteins by OxyBlot analysis. (G) Representative DHE-stained images showing ROS generation in each condition. (H) Images showing cell transfected with ER-targeted HyPer-Red (HyPer-Red ER) in each condition (scale bars, 20 μm). Data are mean ± standard deviation. $^{\#}$, $p < 0.05$; *, $p \leq 0.01$. (For interpretation of the references to colour in this figure legend, the reader is referred to the Web version of this article.)

the ER stress response was increased in D-gal treatment as compared with control (Supplementary Figs. S4A and B). Treatment of GKT or 4-PBA reversed this effect. However, high-dose D-gal treatment for 8–12 h increased the IRE1α-mediated response as indicated by IRE1α phosphorylation and XBP-1 mRNA splicing, but the level of IRE1α phosphorylation, XBP-1 mRNA splicing decreased after chronic stress from D-gal (Fig. 4A and B). To clarify the mechanism underlying canonical and non-canonical IRE1α activation by D-gal-induced senescence, IRE1α oligomerization was visualized using IRE1α-GFP fusion protein, in which green fluorescent protein (GFP) was inserted between the transmembrane and kinase region of IRE1α [44]. The formation of foci-like structures by IRE1α-GFP was more efficient and prolonged with 50 mM D-gal treatment; the formation was attenuated in a high concentration of 200 mM or chronic D-gal treatment in HUVECs (Fig. 4C and D, and Supplementary Fig. S4C). After observing the relationship between ER stress and Nox4-derived ROS in vascular senescence, we next investigated whether Noxs are involved in activation of the ER stress response. Under Nox activation, ROS is suggested to influence signaling molecules through post-translational oxidative modification of proteins [13]. Specifically, Nox-derived ROS, through oxidation of cysteine thiols, is also suggested to alter phosphorylation of the representative UPR sensor IRE1α. After confirming that ROS exposure acutely inhibits the canonical UPR activity of IRE1α, we investigated whether IRE1α is modified by ROS. The initial step in cysteine oxidation of IRE1α is the conversion of the thiol group (SH) to sulfonic acid group (SO_3H). For sulfonylated IRE1α identification, we were analyzed by using the MALDI MS (Supplementary Fig. S5) and we discovered that IRE1α is irreversibly sulfonylated (IRE1α:SO_3H) by dose-dependent D-gal-generated ROS with the extent of sulfonation peaking at around 8 h or 12 h (Fig. 4E and F, and Supplementary Figs. S4D, E, and S5). The increased ROS levels with Nox4 in D-gal induced vascular senescence are favoring irreversible oxidative modifications of IRE1α. Consistently, HyPer-Red ER and protein oxidation levels were increased at 24 h following D-gal treatment (Fig. 4G and H). To confirm the PDI redox status, lysates were exposed to varying times of treatment using diamide oxidative agent. The oxidized form of PDI was readily recovered in reduced form of PDI under short time conditions but persisted in chronic time of D-gal exposed condition (Fig. 4I).

3.5. *IRE1α physically interacts with Nox4 and controls NO bioavailability in D-gal-induced endothelial senescence*

Nox enzymes represent a potential source of inducible ROS production. These enzymes generate superoxide anions by reducing NADPH, in the ER and are present in membrane structures [5]. Nox4 may directly convert superoxide to hydrogen peroxide [27]. To explore the possible function of IRE1α as a scaffold that may dock the Nox4 at ER, we tested the physical association between the two proteins by carrying out immunoprecipitation experiments, which indicated a positive interaction between the proteins (Fig. 5A and B). We also performed proximity ligation assay (PLA) experiments and confirmed the proximity between IRE1α and Nox4 in HUVECs (Fig. 5C and D). The interaction between the IRE1α and Nox4 in the D-gal-induced endothelial senescence was terminated in the presence of GKT or 4-PBA, as determined with the PLA. Thus, in conclusion, D-gal causes stress that leads to activation of Nox4 at or near the ER, leading to ROS production, suggesting that these ROS activate sulfonylated cysteine of IRE1α.

Next, we investigated sites to identify the sulfonylated cysteine in

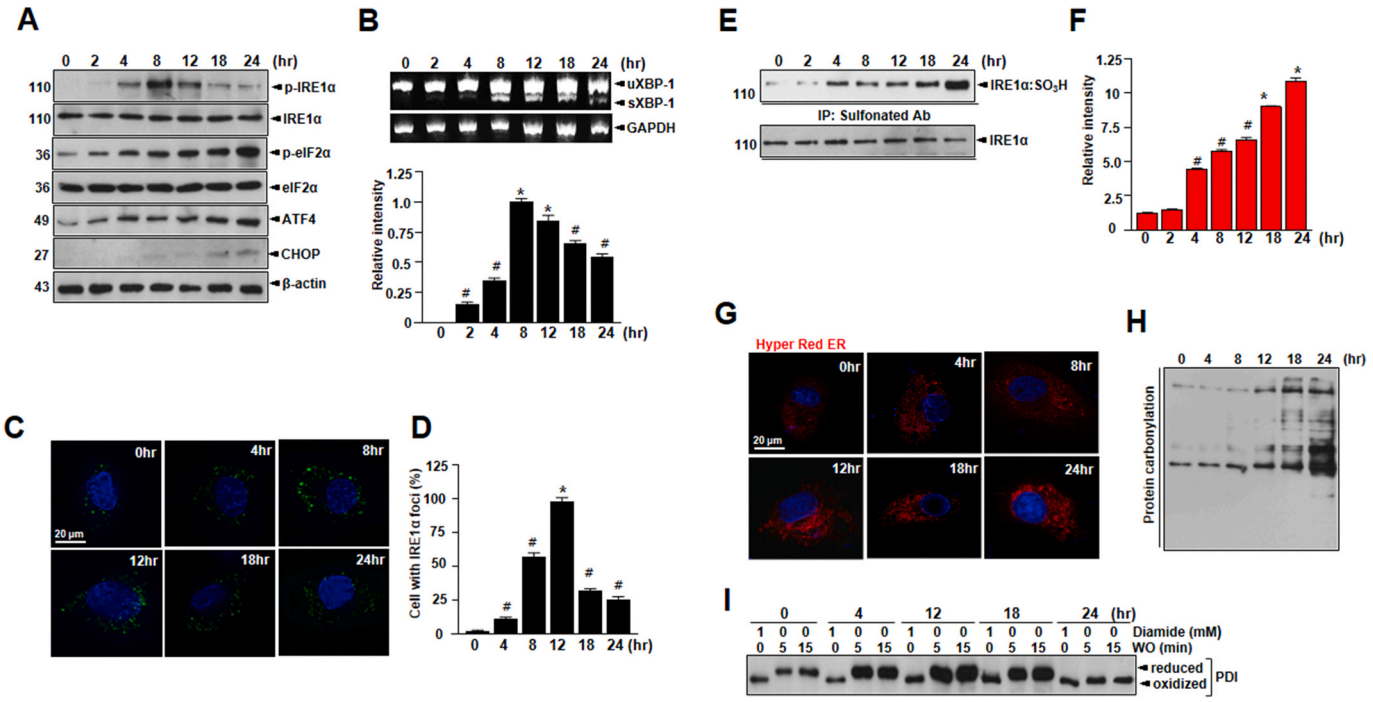

Fig. 4. NADPH oxidase activity in ER fraction accelerates vascular aging and senescence by D-gal-induced oxidative stress and endothelial dysfunction. HUVECs were exposed to 200 mM D-gal for indicated times. (A) Western blots of p-IRE1α, IRE1α, *p*-eIF2α, eIF2α, ATF4, CHOP, and β-actin expression in HUVECs. (B) Total RNA was extracted from the cells and the mRNA of sXBP-1 was detected and analyzed by RT-PCR. The RT-PCR products were analyzed by agarose gel electrophoresis. GAPDH was used as internal control. (C) HUVECs were transfected with IRE1α-GFP expression vector for 24 h prior to D-gal treatment. (D) Percentages of cells with IRE1α foci were calculated by visual inspection in each independent experiment. Irreversible sulfonation (E) of IRE1α was analyzed as described in materials and methods. (F) Quantification of the levels of sulfonation of IRE1α is shown. (G) Images showing cell transfected with ER-targeted HyPer-Red (HyPer-Red ER) for indicated times after the treatment of D-gal. (H) Lysates from lung tissues were analyzed for the presence of oxidized proteins by OxyBlot analysis. (I) Lysates treated with 1 mM diamide or left untreated for 15 min. After washout for the indicated time, the reduced and oxidized forms of PDI were detected by immunoblotting. Scale bars, 20 μm. Data are mean ± standard deviation. $^{\#}$, $p < 0.05$; *, $p \leq 0.01$. (For interpretation of the references to colour in this figure legend, the reader is referred to the Web version of this article.)

IRE1α. C663 located within the activation loop of the IRE1α kinase domain in *C. elegans* is sulfenlyated in a previous report [45] and matched to C715 in human IRE1α (Fig. 5E). Additionally, we found Cys762 another conserved site at the IRE1α kinase domain in humans through alignment of IRE1α amino acid sequences. Thus, we constructed mutated of two cysteine residues of IRE1α to serine. Cells transfected with IRE1α WT revealed increased sulfonation by D-gal, but not by mutant IRE1α C715S/C762S (Fig. 5F). IRE1α sulfonation was decreased in cells transfected with IRE1α C715S, C762S, or C715S/C762S compared to IRE1α WT. However, cells transfected with IRE1α K599A showed increased sulfonation as compared to IRE1α WT with treatment of D-gal, indicating sulfonation of IRE1α by D-gal is independent of phosphorylation of IRE1α (Fig. 5F). The phosphorylation of eNOS Ser1177 level was significantly decreased in IRE1α WT, but not by mutant IRE1α C715S/C762S (Fig. 5G). However, cells transfected with IRE1α K599A showed decreased phosphorylation of eNOS Ser1177 as compared to mutant IRE1α C715S/C762S.

3.6. *Nox4 deficiency in cultured endothelial cells improves vascular function in D-gal-induced endothelial senescence*

To demonstrate the involvement of Nox4 in D-gal-induced endothelial senescence, Nox4 available RNA interference (RNAi) was applied to the current study. Nox4 protein expression was decreased in cells from Nox4 siRNA-transduced cells (Fig. 6A). SA-β-gal, a biomarker of cell-senescence, was significantly decreased in Nox4-silenced cells as compared to scrambled siRNA-transduced cells (Fig. 6B). The expression of phosphorylation of eNOS Ser1177 and NO production were increased in Nox4-silenced cells (Fig. 6C and D). Also, ROS production was lower in Nox4-silenced cells (Fig. 6E). ER-generated ROS, NADPH oxidase, and H_2O_2 were decreased in Nox4-silenced cells as compared to the control (Fig. 6F–H). The sulfonated cysteine in IRE1α was decreased in Nox4-silenced cells (Fig. 6I). These data support the potential role of Nox4 depletion in aging-induced human vascular dysfunction.

3.7. *Nox4 overexpression exacerbates vascular function in cultured endothelial cells*

HUVECs were transfected with pcDNA vector expressing complete human Nox4 cDNA in order to determine whether the over-expression of exogenous Nox4 regulated vascular function, (Fig. 7A). SA-β-gal was increased in Nox4-overexpressing cells compared with Nox4 siRNA-transduced cells (Fig. 7B). The expression of phosphorylated eNOSSer1177 and NO production were decreased in Nox4-overexpressing cells (Fig. 7C and D). Also, ROS production was higher in Nox4-overexpressing cells (Fig. 7E). ER-generated ROS, NADPH oxidase, and H_2O_2 were increased in Nox4-overexpressing cells compared with Nox4 siRNA cells (Fig. 7F–H). The sulfonated cysteine in IRE1α was increased in Nox4-overexpressing cells (Fig. 7I). Collectively, these results indicate the regulatory role of Nox4 in human vascular function.

4. Discussion

In this study, Nox4 and ER-originated ROS were examined based upon nitric oxide-associated aorta function. The alterations of eNOS Ser phosphorylation which are linked to aortic contractility explain that the Nox4-ROS-IRE1α axis is the main signaling axis to explain age-dependent vascular dysfunction. Especially, the post-modification of

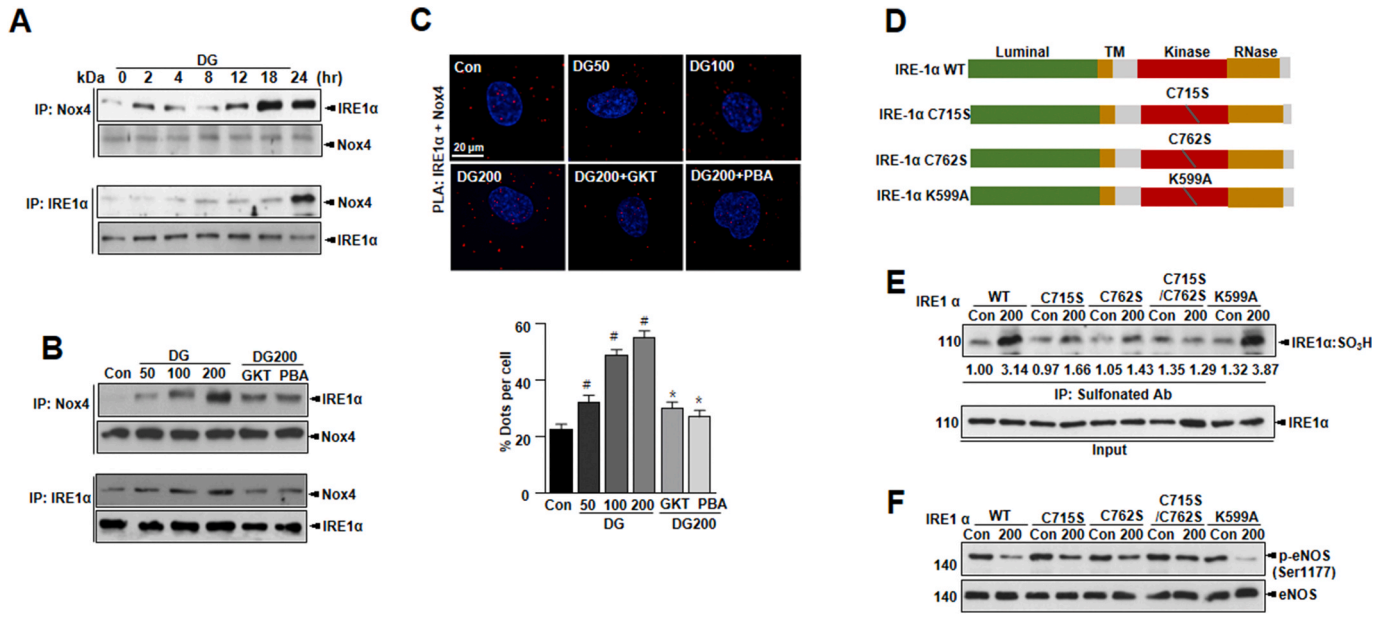

Fig. 5. IRE1α physically interacts with Nox4 and controls NO bioavailability in D-gal-induced endothelial senescence. Lysates were immunoprecipitated and immunoblotted with *anti*-Nox4 antibody and immunoblotted with anti-IRE1α antibody for indicated times (A) and dose (B). The proximity ligation assay (PLA) assay with fluorescence images of HUVECs are shown (C). Quantification of the number of positive PLA dots per cell (Nox4 and IRE1α interactions) are shown for indicated samples. (D) Schematic of IRE1α structure and the mutants analyzed (TM; transmembrane domain). (E) Immunoprecipitation using anti-sulfonate antibody was conducted in cells with transiently transfected IRE1α wild type (WT) and IRE1α mutant plasmid tagging to flag (C715S/C762S, C762S, C715S, and K599A). (F) Western blots of *anti*-phospho-eNOS Ser1177 or total-eNOS antibody were performed in cells transiently transfected with IRE1α wild type (WT) and IRE1α mutant plasmid tagging to flag (C715S/C762S, C762S, C715S, and K599A). Scale bars, 20 μm. Data are mean ± standard deviation. #, $p < 0.05$; *, $p \leq 0.01$.

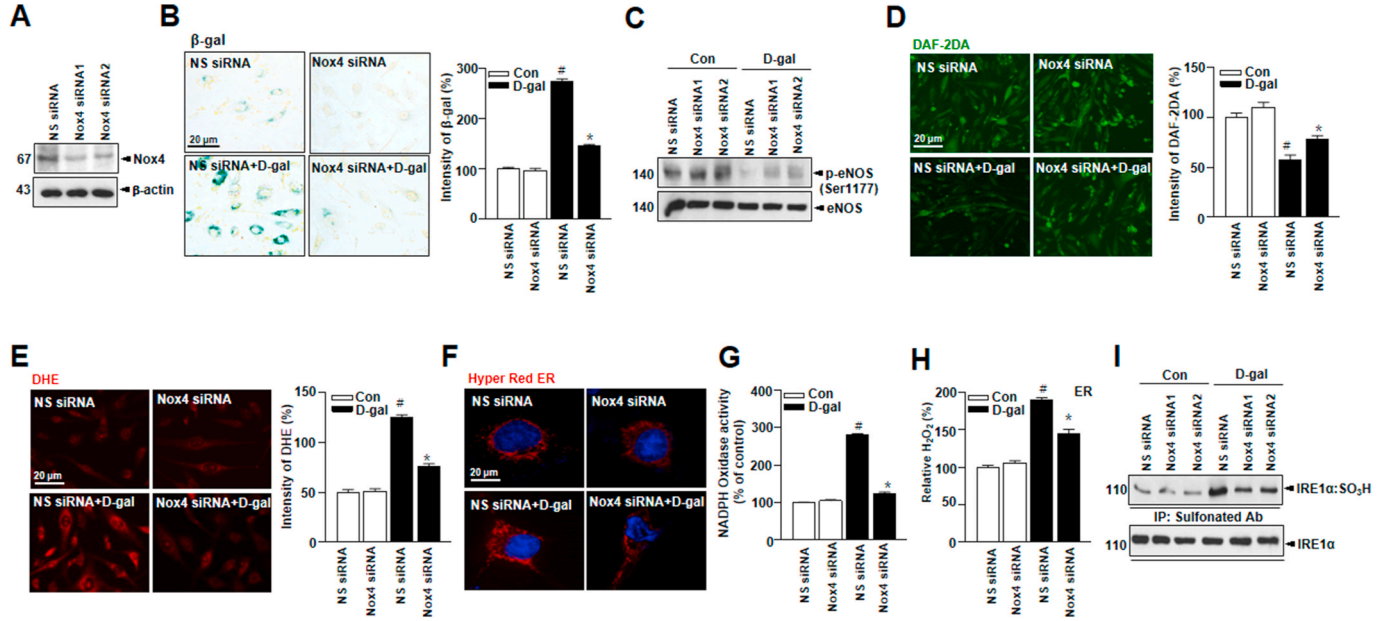

Fig. 6. Nox4 deficiency in cultured endothelial cells improves vascular function in D-gal-induced endothelial senescence. (A) HUVECs were transiently transfected with Nox4 siRNA, followed by transfection with pcDNA-Nox4 or empty vector. (B) Representative senescence-associated β-galactosidase (SA-β-gal) staining in HUVECs. (C) Western blots analysis of *anti*-phospho-eNOS Ser1177 or total-eNOS antibody. (D) Representative fluorescent images of NO formation in HUVECs were shown using NO probe DAF-2DA. (E) Representative cells were stained for DHE. (F) Images showing cell transfected with ER-targeted HyPer-Red (HyPer Red ER). ER NADPH oxidase activity (G) and hydrogen peroxide level (H) were measured in HUVECs. (I) Irreversible sulfonation of IRE1α was analyzed with transiently transfected with non-specific-siRNA or Nox4 siRNA. Scale bars, 20 μm. Data are mean ± standard deviation. #, $p < 0.05$; *, $p \leq 0.01$. (For interpretation of the references to colour in this figure legend, the reader is referred to the Web version of this article.)

IRE1α, including IRE1α phosphorylation or sulfonation is critical signal to determine "adaptation or maladaptation" in aging process, ultimately suggesting that our findings identify the interplay between oxidative stress and ER stress response as a novel molecular mechanism underlying vascular dysfunction in the aging process.

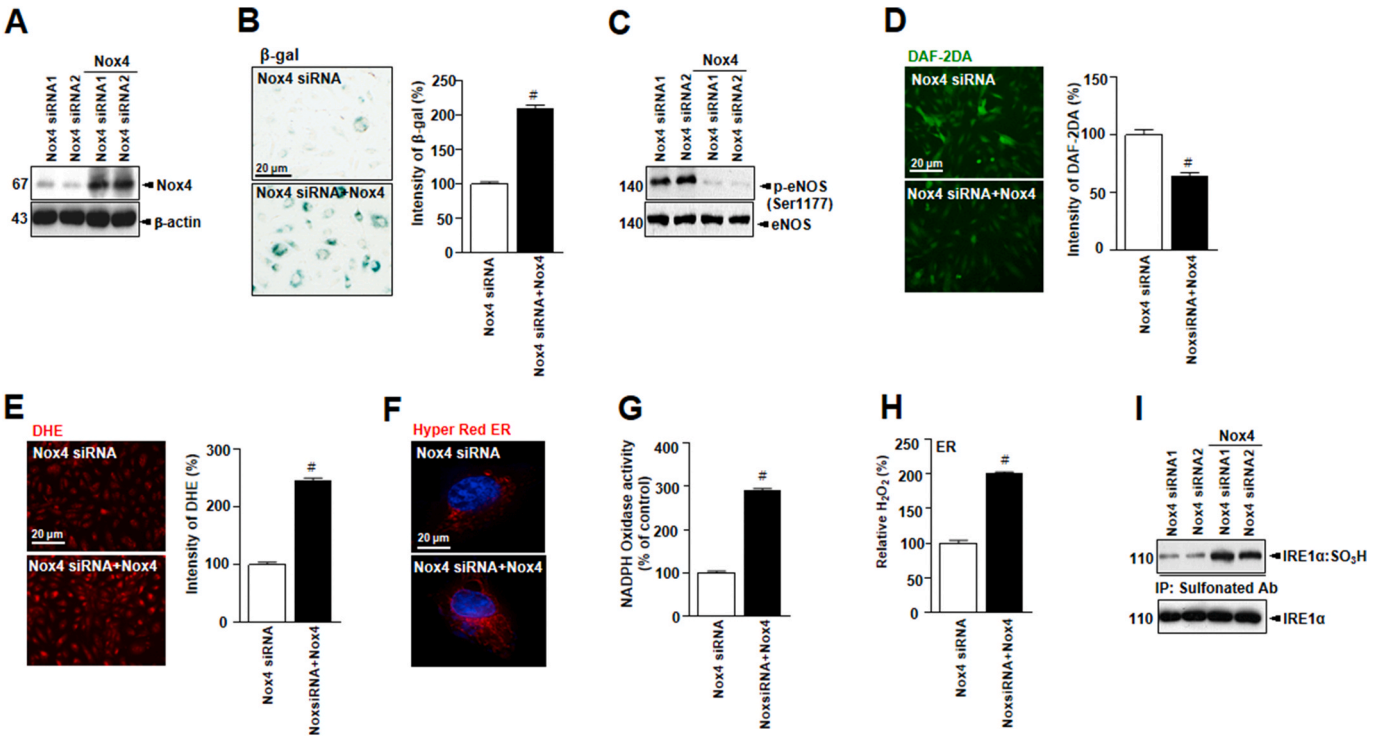

Fig. 7. Nox4 overexpression in cultured endothelial cells suppresses vascular function in endothelial senescence. (A)HUVECs were transiently transfected with non-specific siRNA or Nox4 siRNA, followed by transfection with pcDNA-Nox4 or empty vector. (B) Representative senescence-associated β-galactosidase (SA-β-gal) staining in HUVECs. (C) Western blots of *anti*-phospho-eNOS Ser1177 or total-eNOS antibody. (D) Representative fluorescent images of NO formation in HUVECs are shown using the NO probe DAF-2DA. (E) Representative aortic sections were stained for DHE. (F) Images showing cells transfected with ER-targeted HyPer-Red (HyPer Red ER). ER NADPH oxidase activity (G) and hydrogen peroxide levels (H) in HUVECs were measured. (I) Irreversible sulfonylation of IRE1α was analyzed by western blots. Scale bars, 20 μm. Data represent mean ± standard deviation. #, $p < 0.05$; *, $p \leq 0.01$. (For interpretation of the references to colour in this figure legend, the reader is referred to the Web version of this article.)

4.1. The role of ROS in eNOS uncoupling-associated vascular aging

Our findings suggest that Nox4 abundance alters the function of eNOS, resulting in diminishing NO production and increasing production of ROS in aging condition. Nox is critically important in producing ROS, ultimately oxidizing vascular controlling proteins in aging vascular system [46]. In the present study, we disclosed a functional link between Nox4 and eNOS dysfunction/decrease in NO bioavailability *in vivo* in young and aged Nox4 WT mice model (Fig. 2B and C) as well as in cultured HUVECs exposed to D-gal (Fig. 3D and E). Our findings identify Nox4 as a pivotal mediator of aging-induced eNOS dysfunction and strongly suggest that the molecular mechanisms underlying this process may involve reaction of Nox4-derived superoxide with NO generated constitutively by functional eNOS, resulting in the formation of uncoupling eNOS, further promoting superoxide generation. Our previous studies also suggest that there is an important interaction between this oxidase and eNOS, whereby increased production of ROS by the former impairs NO production and stimulates the production of ROS by the latter [47]. The role of superoxide anion, which is produced by the Nox, in vascular disease is widely accepted [46,48]. Among the various homologues of the enzyme serving different functions in physiology and pathology [48,49], the mainly ER-localized Nox4 is suggested to contribute to oxidant stress by producing superoxide, leading to eNOS uncoupling in vascular system in this study. The combination of reduced NO and increased ROS production may not only contribute to the disturbance of vascular contraction/relaxation system. Similarly, NADPH oxidases family has been proposed to be the source of kindling radicals that contribute to initiating eNOS dysfunction [50].

4.2. The meaning of IRE1α phosphorylation-XBP-1 splicing and IRE1α sulfonation in aging process

Our findings suggest that Nox4 abundance alters the function of eNOS, resulting in diminished NO production and increased ROS production in aging condition. NADPH oxidase is critically important in producing ROS which ultimately oxidizes vascular controlling proteins in blood vessels of aging animals [51]. Among the oxidases, Nox4 mainly localizes at ER membrane, interacting with some critical signaling proteins contributing to ER redox balance (Fig. 1E) [5]. In the present study, we exposed a functional link between Nox4 and eNOS dysfunction/decrease in NO bioavailability *in vivo* in young and aged Nox4 WT mice models (Fig. 2B and C) as well as in cultured HUVECs exposed to D-gal (Fig. 3D and E), suggesting that the molecular mechanisms underlying this process may involve reaction of Nox4-derived superoxide with NO generated constitutively by functional eNOS, resulting in the formation of uncoupled eNOS, further promoting superoxide generation. Furthermore, the functional significance of Nox4 in ER may highlight crosstalk between oxidative stress and ER stress as previously suggested [52]. Altered ER function and activation of the UPR triggers ER stress, leading to inflammation, abnormal cell growth and apoptosis. ER stress, which is redox sensitive, is triggered by altered ER function and activation of the UPR, leading to abnormal cell growth, apoptosis, and inflammation [11]. ER stress also promotes oxidative stress and ROS production. Our data found that Nox4 specifically oxidizes the ER membrane-associated ER stress sensor, IRE1α. The IRE1α is composed of an endoribonuclease domain and a kinase domain. Under stress, IRE1α cleaves XBP1, leading to splicing of active transcription factor sXBP1, finally linking to the role of ER homeostasis and cell survival. For ER homeostasis, ER stress triggers UPR, including the IRE1α-XBP1 axis (survival pathway), which is connected with

upregulation of ER-derived chaperones and folding enzymes for degradation of unfolded proteins [53]. Under chronic/severe stress, IRE1α kinase activates ASK1-JNK (apoptosis signal-regulating kinase 1-*c*-Jun N-terminal kinase) pathway, resulting in ER dysfunction and cell death [11]. This study also focused on the criteria to determine adaptation and maladaption, showing reduced/altered function of protein folding capacity in the aging condition. Exposed to high levels of ROS, further oxidation of cysteine S-sulfenylation can occur, leading to formation of sulfonic acid (-SO_3H), one of the irreversible types of oxidation, rather than cleaves XBP1 through IRE1α. Considered that sulfenylation of IRE1α induces the p38/Nrf2 antioxidant signaling and cell protection [45], the transient and reversible post-translational modification was not critically studied here instead, the relatively stable modification was in depth showed in this study.

Although the luminal domain of overexpressed IRE1α forms a dimer by hydrophobic interaction that is stabilized by intermolecular disulfide bridges between Cys148 and Cys332 [54], these cysteines are not necessary for stress signaling sensor of IRE1α [54]. ER redox imbalance-based IRE1α cysteine sulfonation happens in cytosol site finally leading to vascular dysfunction without XBP-1 splicing whereas PDIA6 regulate IRE1α signaling including IRE1α phosphorylation and XBP-1 splicing through the intermolecular disulfide bridges between Cys148 and Cys332 from the luminal domain. The two signaling "IRE1α phosphorylation-XBP-1 splicing and ROS-IRE1α sulfonation" independently work each other, explaining the detrimental effect on the vascular function representatively eNOS coupling.

Next, this study determines whether Nox4-drived ROS induces IRE1α oxidation or IRE1α phosphorylation-activation of XBP1 under stress. The phosphorylation of IRE1α and splicing of XBP1 are increased in low-dose D-gal treatment and sulfonation of IRE1α is increased in long time or high-dose D-gal treatment, which is reversed by GKT137831 and 4-PBA (Fig. 4 and Supplementary Fig. S4). This study suggests that Nox4 and ER stress determine the direction of adaptation or maladaptation in endothelial aging phenomena.

4.3. The IRE1α sulfonation is related with Nox4 activity in aging-associated vascular dysfunction

In vascular system, Nox4 is constitutively activated and it primarily produces superoxide and the linked H_2O_2, and its interaction with other proteins, including IRE1α is also focused in vascular signaling process. Under high expression of ER-localized Nox4, high ROS accumulation stimulated IRE1α sulfonation, ultimately leading to vascular dysfunction in aged conditions (Fig. 5). Considering that IRE1α sulfenylation and the subsequent sulfonation are related to ROS [45,55], ER-localized Nox4, and the associated ER stress sensor, IRE1α sulfonation seems to contribute to ER redox imbalance-based vascular dysfunction in aging process. ER-originated ROS, not mitochondria-originated ROS is the main explanation for the IRE1α sulfonation due to the subcellular localization of Nox4 (Fig. 1D), however the ER-connected mitochondria ROS axis might contribute to the IRE1α modification.

This study suggests that the interaction of IRE1α with Nox4 is one of the mechanisms to explain the relation of Nox4-IRE1α-eNOS axis in the aging-associated vascular dysfunction.

In conclusion, the Nox4 activity-based IRE1α phosphorylation-XBP-1 axis and IRE1α sulfonation state are explaining vascular function state in aging process. The increased eNOS uncoupling, a representative mechanism to explain vascular dysfunction, is due to the ER stress-maladaptation condition showing over the threshold of functional resistance against ROS and the irreversible oxidation, "IRE1α sulfonation". Nox4-IRE1α status is explaining the aging-associated vascular dysfunction, opening the possibility of a potential anti-aging or anti-cardiovascular dysfunctional strategy.

Declaration of compting interest

The authors declare that they have no known competing financial interests or personal relationships that could have appeared to influence the work reported in this paper.

Acknowledgments

This research was supported by the National Research Foundation of Korea (NRF), Republic of Korea (NRF-2018R1D1A3B07049580, 2017R1E1A1A01073796 and 2017M3A9G7072719).

Appendix A. Supplementary data

Supplementary data to this article can be found online at https://doi.org/10.1016/j.redox.2020.101727.

References

[1] B. Reissmann, T. Budelmann, E. Wissner, M. Schluter, C.H. Heeger, S. Mathew, T. Maurer, C. Lemes, T. Fink, A. Rillig, F. Santoro, J. Riedl, F. Ouyang, K.H. Kuck, A. Metzner, Five-year clinical outcomes of visually guided laser balloon pulmonary vein isolation for the treatment of paroxysmal atrial fibrillation, Clin. Res. Cardiol. 107 (5) (2018) 405–412.
[2] M. Gerhard, M.A. Roddy, S.J. Creager, M.A. Creager, Aging progressively impairs endothelium-dependent vasodilation in forearm resistance vessels of humans, Hypertension 27 (4) (1996) 849–853.
[3] K.H. Krause, Aging: a revisited theory based on free radicals generated by NOX family NADPH oxidases, Exp. Gerontol. 42 (4) (2007) 256–262.
[4] A.C. Montezano, S. Tsiropoulou, M. Dulak-Lis, A. Harvey, L. Camargo Lde, R. M. Touyz, Redox signaling, Nox5 and vascular remodeling in hypertension, Curr. Opin. Nephrol. Hypertens. 24 (5) (2015) 425–433.
[5] F.R. Laurindo, T.L. Araujo, T.B. Abrahao, Nox NADPH oxidases and the endoplasmic reticulum, Antioxidants Redox Signal. 20 (17) (2014) 2755–2775.
[6] R.V. Rao, D.E. Bredesen, Misfolded proteins, endoplasmic reticulum stress and neurodegeneration, Curr. Opin. Cell Biol. 16 (6) (2004) 653–662.
[7] M.K. Brown, N. Naidoo, The endoplasmic reticulum stress response in aging and age-related diseases, Front. Physiol. 3 (2012) 263.
[8] S.K. Bardaweel, M. Gul, M. Alzweiri, A. Ishaqat, A.L. Ha, R.M. Bashatwah, Reactive oxygen species: the dual role in physiological and pathological conditions of the human body, Eurasian J Med 50 (3) (2018) 193–201.
[9] J. Hong, K. Kim, J.H. Kim, Y. Park, The role of endoplasmic reticulum stress in cardiovascular disease and exercise, Int J Vasc Med 2017 (2017) 2049217.
[10] K.R. Bohnert, J.D. McMillan, A. Kumar, Emerging roles of ER stress and unfolded protein response pathways in skeletal muscle health and disease, J. Cell. Physiol. 233 (1) (2018) 67–78.
[11] S.S. Cao, R.J. Kaufman, Endoplasmic reticulum stress and oxidative stress in cell fate decision and human disease, Antioxidants Redox Signal. 21 (3) (2014) 396–413.
[12] A. Gorlach, K. Bertram, S. Hudecova, O. Krizanova, Calcium and ROS: a mutual interplay, Redox Biol 6 (2015) 260–271.
[13] C.C. Winterbourn, M.B. Hampton, Thiol chemistry and specificity in redox signaling, Free Radic. Biol. Med. 45 (5) (2008) 549–561.
[14] L.B. Poole, K.J. Nelson, Discovering mechanisms of signaling-mediated cysteine oxidation, Curr. Opin. Chem. Biol. 12 (1) (2008) 18–24.
[15] K. Niforou, C. Cheimonidou, I.P. Trougakos, Molecular chaperones and proteostasis regulation during redox imbalance, Redox Biol 2 (2014) 323–332.
[16] B. D'Autreaux, M.B. Toledano, ROS as signalling molecules: mechanisms that generate specificity in ROS homeostasis, Nat. Rev. Mol. Cell Biol. 8 (10) (2007) 813–824.
[17] S.S. Cao, R.J. Kaufman, Unfolded protein response, Curr. Biol. 22 (16) (2012) R622–R626.
[18] S.H. Back, R.J. Kaufman, Endoplasmic reticulum stress and type 2 diabetes, Annu. Rev. Biochem. 81 (2012) 767–793.
[19] S. Wang, R.J. Kaufman, The impact of the unfolded protein response on human disease, J. Cell Biol. 197 (7) (2012) 857–867.
[20] A.M. Faria, A. Papadimitriou, K.C. Silva, J.M. Lopes de Faria, J.B. Lopes de Faria, Uncoupling endothelial nitric oxide synthase is ameliorated by green tea in experimental diabetes by re-establishing tetrahydrobiopterin levels, Diabetes 61 (7) (2012) 1838–1847.
[21] C.E. Paulsen, T.H. Truong, F.J. Garcia, A. Homann, V. Gupta, S.E. Leonard, K. S. Carroll, Peroxide-dependent sulfenylation of the EGFR catalytic site enhances kinase activity, Nat. Chem. Biol. 8 (1) (2011) 57–64.
[22] N.K. Tonks, Redox redux: revisiting PTPs and the control of cell signaling, Cell 121 (5) (2005) 667–670.
[23] Z. Xue, Y. He, K. Ye, Z. Gu, Y. Mao, L. Qi, A conserved structural determinant located at the interdomain region of mammalian inositol-requiring enzyme 1alpha, J. Biol. Chem. 286 (35) (2011) 30859–30866.
[24] H. ten Freyhaus, M. Huntgeburth, K. Wingler, J. Schnitker, A.T. Baumer, M. Vantler, M.M. Bekhite, M. Wartenberg, H. Sauer, S. Rosenkranz, Novel Nox

inhibitor VAS2870 attenuates PDGF-dependent smooth muscle cell chemotaxis, but not proliferation, Cardiovasc. Res. 71 (2) (2006) 331–341.
[25] M.R. Wieckowski, C. Giorgi, M. Lebiedzinska, J. Duszynski, P. Pinton, Isolation of mitochondria-associated membranes and mitochondria from animal tissues and cells, Nat. Protoc. 4 (11) (2009) 1582–1590.
[26] Z. Ungvari, S. Tarantini, A.J. Donato, V. Galvan, A. Csiszar, Mechanisms of vascular aging, Circ. Res. 123 (7) (2018) 849–867.
[27] Y. Nisimoto, B.A. Diebold, D. Cosentino-Gomes, J.D. Lambeth, Nox4: a hydrogen peroxide-generating oxygen sensor, Biochemistry 53 (31) (2014) 5111–5120.
[28] T. Minamino, H. Miyauchi, T. Yoshida, Y. Ishida, H. Yoshida, I. Komuro, Endothelial cell senescence in human atherosclerosis: role of telomere in endothelial dysfunction, Circulation 105 (13) (2002) 1541–1544.
[29] J. Schwendemann, B. Sehringer, C. Noethling, H.P. Zahradnik, W.R. Schaefer, Nitric oxide detection by DAF (diaminofluorescein) fluorescence in human myometrial tissue, Gynecol. Endocrinol. 24 (6) (2008) 306–311.
[30] R. Rafikov, F.V. Fonseca, S. Kumar, D. Pardo, C. Darragh, S. Elms, D. Fulton, S. M. Black, eNOS activation and NO function: structural motifs responsible for the posttranslational control of endothelial nitric oxide synthase activity, J. Endocrinol. 210 (3) (2011) 271–284.
[31] A.G. Rajapakse, G. Yepuri, J.M. Carvas, S. Stein, C.M. Matter, I. Scerri, J. Ruffieux, J.P. Montani, X.F. Ming, Z. Yang, Hyperactive S6K1 mediates oxidative stress and endothelial dysfunction in aging: inhibition by resveratrol, PloS One 6 (4) (2011), e19237.
[32] A.A. Eid, D.Y. Lee, L.J. Roman, K. Khazim, Y. Gorin, Sestrin 2 and AMPK connect hyperglycemia to Nox4-dependent endothelial nitric oxide synthase uncoupling and matrix protein expression, Mol. Cell Biol. 33 (17) (2013) 3439–3460.
[33] C. Urso, G. Caimi, [Oxidative stress and endothelial dysfunction], Minerva Med. 102 (1) (2011) 59–77.
[34] E.D. Yoboue, R. Sitia, T. Simmen, Redox crosstalk at endoplasmic reticulum (ER) membrane contact sites (MCS) uses toxic waste to deliver messages, Cell Death Dis. 9 (3) (2018) 331.
[35] A.J. Donato, R.G. Morgan, A.E. Walker, L.A. Lesniewski, Cellular and molecular biology of aging endothelial cells, J. Mol. Cell. Cardiol. 89 (Pt B) (2015) 122–135.
[36] B.P. Tu, J.S. Weissman, Oxidative protein folding in eukaryotes: mechanisms and consequences, J. Cell Biol. 164 (3) (2004) 341–346.
[37] V.V. Belousov, A.F. Fradkov, K.A. Lukyanov, D.B. Staroverov, K.S. Shakhbazov, A. V. Terskikh, S. Lukyanov, Genetically encoded fluorescent indicator for intracellular hydrogen peroxide, Nat. Methods 3 (4) (2006) 281–286.
[38] M. Forkink, G.R. Manjeri, D.C. Liemburg-Apers, E. Nibbeling, M. Blanchard, A. Wojtala, J.A. Smeitink, M.R. Wieckowski, P.H. Willems, W.J. Koopman, Mitochondrial hyperpolarization during chronic complex I inhibition is sustained by low activity of complex II, III, IV and V, Biochim. Biophys. Acta 1837 (8) (2014) 1247–1256.
[39] M. Forkink, F. Basit, J. Teixeira, H.G. Swarts, W.J.H. Koopman, P. Willems, Complex I and complex III inhibition specifically increase cytosolic hydrogen peroxide levels without inducing oxidative stress in HEK293 cells, Redox Biol 6 (2015) 607–616.
[40] X. Zhang, C.S. Gibhardt, T. Will, H. Stanisz, C. Korbel, M. Mitkovski, I. Stejerean, S. Cappello, D. Pacheu-Grau, J. Dudek, N. Tahbaz, L. Mina, T. Simmen, M. W. Laschke, M.D. Menger, M.P. Schon, V. Helms, B.A. Niemeyer, P. Rehling, A. Vultur, I. Bogeski, Redox signals at the ER-mitochondria interface control melanoma progression, EMBO J. 38 (15) (2019), e100871.
[41] C. Appenzeller-Herzog, Glutathione- and non-glutathione-based oxidant control in the endoplasmic reticulum, J. Cell Sci. 124 (Pt 6) (2011) 847–855.
[42] C. Appenzeller-Herzog, J. Riemer, E. Zito, K.T. Chin, D. Ron, M. Spiess, L. Ellgaard, Disulphide production by Ero1alpha-PDI relay is rapid and effectively regulated, EMBO J. 29 (19) (2010) 3318–3329.
[43] M.D. Herrera, C. Mingorance, R. Rodriguez-Rodriguez, M. Alvarez de Sotomayor, Endothelial dysfunction and aging: an update, Ageing Res. Rev. 9 (2) (2010) 142–152.
[44] H. Li, A.V. Korennykh, S.L. Behrman, P. Walter, Mammalian endoplasmic reticulum stress sensor IRE1 signals by dynamic clustering, Proc. Natl. Acad. Sci. U. S. A. 107 (37) (2010) 16113–16118.
[45] J.M. Hourihan, L.E. Moronetti Mazzeo, L.P. Fernandez-Cardenas, T.K. Blackwell, Cysteine sulfenylation directs IRE-1 to activate the SKN-1/Nrf2 antioxidant response, Mol. Cell 63 (4) (2016) 553–566.
[46] A. Konior, A. Schramm, M. Czesnikiewicz-Guzik, T.J. Guzik, NADPH oxidases in vascular pathology, Antioxidants Redox Signal. 20 (17) (2014) 2794–2814.
[47] H.Y. Lee, H.M.A. Zeeshan, H.R. Kim, H.J. Chae, Nox4 regulates the eNOS uncoupling process in aging endothelial cells, Free Radic. Biol. Med. 113 (2017) 26–35.
[48] A. Nguyen Dinh Cat, A.C. Montezano, D. Burger, R.M. Touyz, Angiotensin II, NADPH oxidase, and redox signaling in the vasculature, Antioxidants Redox Signal. 19 (10) (2013) 1110–1120.
[49] K. Schroder, M. Zhang, S. Benkhoff, A. Mieth, R. Pliquett, J. Kosowski, C. Kruse, P. Luedike, U.R. Michaelis, N. Weissmann, S. Dimmeler, A.M. Shah, R.P. Brandes, Nox4 is a protective reactive oxygen species generating vascular NADPH oxidase, Circ. Res. 110 (9) (2012) 1217–1225.
[50] R.S. Frey, M. Ushio-Fukai, A.B. Malik, NADPH oxidase-dependent signaling in endothelial cells: role in physiology and pathophysiology, Antioxidants Redox Signal. 11 (4) (2009) 791–810.
[51] S. Sahoo, D.N. Meijles, P.J. Pagano, NADPH oxidases: key modulators in aging and age-related cardiovascular diseases? Clin. Sci. (Lond.) 130 (5) (2016) 317–335.
[52] C.X. Santos, A.A. Nabeebaccus, A.M. Shah, L.L. Camargo, S.V. Filho, L.R. Lopes, Endoplasmic reticulum stress and Nox-mediated reactive oxygen species signaling in the peripheral vasculature: potential role in hypertension, Antioxidants Redox Signal. 20 (1) (2014) 121–134.
[53] C. Hetz, B. Mollereau, Disturbance of endoplasmic reticulum proteostasis in neurodegenerative diseases, Nat. Rev. Neurosci. 15 (4) (2014) 233–249.
[54] C.Y. Liu, Z. Xu, R.J. Kaufman, Structure and intermolecular interactions of the luminal dimerization domain of human IRE1alpha, J. Biol. Chem. 278 (20) (2003) 17680–17687.
[55] L.L. Camargo, A.P. Harvey, F.J. Rios, S. Tsiropoulou, R.N.O. Da Silva, Z. Cao, D. Graham, C. McMaster, R.J. Burchmore, R.C. Hartley, N. Bulleid, A. C. Montezano, R.M. Touyz, Vascular Nox (NADPH oxidase) compartmentalization, protein hyperoxidation, and endoplasmic reticulum stress response in hypertension, Hypertension 72 (1) (2018) 235–246.